Robust Adaptive Control of Manipulators

Kim Doang Nguyen, Harry Dankowicz
Department of Mechanical Science and Engineering
University of Illinois at Urbana-Champaign

January 9, 2014

Abstract

This paper develops an adaptive controller for robot manipulators. The design decouples the system's adaptation and control loops to allow for fast estimation rates, while guaranteeing robustness. The control scheme is tested in different manipulation scenarios, namely, (i) trajectory tracking where the desired joint motions are predefined and (ii) command following where the desired motions are not known a priori and instead inferred using measurements and inverse kinematics. We consider, in addition, an operating modality in which the control scheme switches between command following and static positioning, for which the predefined desired joint motions are constant in time and identical to the manipulator angles at the time of switching. The simulation results illustrate the performance of the proposed control algorithm and its ability to deal with unmodeled dynamics, measurement noise, and time delay, while maintaining smooth control signals.

1 Introduction

Robot manipulators are widely used in industry and have long been considered as testbeds for research in nonlinear control theory. Early work on adaptive control of manipulators was mostly based on model-reference adaptive-control architectures, which drive the system response to a reference model via adaptive estimation of unknown parameters [1, 2, 3]. In [4], the authors present a model-based controller that employs a parameter-adaptation scheme to eliminate the contributions of nonlinearities to the equations of motion governing a robotic arm, and to reject disturbances. However, this control scheme requires acceleration measurements and access to the inverse of the mass matrix. The control architecture in [5], which eliminates those disadvantages, is composed of a proportional-derivative feedback loop together with adaptation laws to compensate for nonlinearities and to estimate the unknown parameters in the system model. The controller exploits the dynamic structure and the passivity property of rigid robot dynamics in the absence of friction. It decouples the nonlinearity into a regression matrix and a vector of unknown parameters and implements an adaptive scheme to estimate these parameters.

The formulation proposed in [5] was further exploited in [6] for the development of repetitive and adaptive control strategies without the need for velocity measurements; in back-stepping design [7]; in the context of adaptive Jacobian tracking [8]; for image-based visual servoing control of manipulators [9]; and for space-robot control with optimal sensor architecture [10]. In these papers, the manipulator control adaptively adjusts the system energy to obtain the control objective, while preserving the passivity of the robotic mechanism. Such a control design philosophy, based on dynamic passivity, led to several important papers in robot control [12, 13, 14, 15, 16, 17]. Disturbance observers were designed for manipulator control in [18, 19, 20, 21]. In these control schemes, the filtered system states are used for the inversion of the robot

dynamics. Joint torques/forces are treated as disturbances and compensated for by the controller design. This eliminates the need for torque/force sensors, while keeping the desirable tracking performance. However, these controllers may suffer from inversion errors, since they perform filtering before plant inversion and therefore require accurate system modeling. A modification to disturbance-observer structure was proposed in [22] to alleviate the dependence on the accuracy of plant modeling. Disturbance observers were also applied with a force estimator in the scenario of human-robot comanipulation [23].

The work in [24] proposed a systematic method for integrating sliding-mode control in a model-reference adaptive controller to drive a robot arm to track certain trajectories. Following this work, robust adaptive control schemes with semi-strict feedback forms were developed for single-input-single-output [25] systems and multi-input-multi-output systems [26]. Recently, sliding-mode control has been employed to design an observer-based adaptive controller for servo actuators with friction. Adaptation laws compensate for the uncertain friction and load torque with the estimated friction state [27]. The main disadvantage of this control formulation comes from the property of the sliding mode: the control law is discontinuous across the sliding surface. In practice, therefore, a resultant chattering control signal may excite unmodeled high-frequency dynamics and seriously damage the system's robustness. The architecture can be modified to improve the robustness, but with the sacrifice of tracking accuracy and asymptotic stability [28, 29]. In addition, the bounds of the unknown parameters and disturbances must be known to design an adaptive sliding-mode controller for robustness and convergence [30].

In the context of robot manipulators, all existing control architectures in the presence of an estimation loop share the structural property that the control loop and the estimation loop are coupled. As a result, in order to maintain desirable performance in the presence of disturbances or unmodeled dynamics, the adaptation rate must be increased. This, in turn, will make the control signal oscillate with high frequency and high amplitude, deteriorating the system's tolerance to time delays [31]. Furthermore, as in [5], it must be possible to decouple the nonlinearities in terms of a matrix product of a regression matrix and a vector of unknown parameters, where the regression matrix is known. Any uncertainty in the dynamic structure or measurement noise will degrade the system performance [32].

The so-called $\mathcal{L}_1$ control architecture has been developed to enable fast adaptation, while guaranteeing robustness with time-delay margin bounded away from zero, as well as maintaining clean control channels [33, 34]. The performance of $\mathcal{L}_1$ control has been demonstrated in numerous aerospace applications [35, 36, 37, 38]. Inspired by this work, this paper proposes a controller for robot manipulators, which does not require measurement of accelerations and eliminates the need to compute the inverse of the inertia matrix. Moreover, a low-pass filter in the feedback channel decouples the estimation loop from the control loop, and with that facilitates the increase of estimation rates without sacrificing robustness. Tuning of the filter also allows for shaping the nominal response and enhancing the time-delay margin.

The adaptive controller is developed for manipulators in two scenarios: 1) tracking predefined joint trajectories and 2) following unknown command movements when interacting with a user. The first task is used to assess the performance of most algorithms for robot control. The second task was studied in [39] and [40] with a hybrid control scheme to make a lower-limb exoskeleton follow human movement while supporting a payload. Unlike that work, the proposed controller in this paper is able to adaptively estimate the robot nonlinearity, which are hard to model, with guaranteed robustness. A switching strategy between these two scenarios is also presented. The control schemes' performance is demonstrated with a typical three-degree-of-freedom robotic arm.

The remainder of this paper is organized as follows. The dynamic model of manipulators is discussed in Sec. 2, in which the robot dynamics is converted to a relevant form. The adaptive controller for manipulators is designed and analyzed in Sec. 3. Section 4 presents the simulation results of a robot arm performing trajectory tracking tasks, including the presence of base-motion disturbances and actuator delay. Section 5

couples the control architecture with an additional estimation loop in order to support the task of command following, and demonstrates this concept in the context of a switching strategy between command following and static positioning, for which the predefined joint trajectory is constant in time. Finally, the paper concludes in Sec. 6 with a discussion.

2 Dynamic Model of Manipulators

Let a superscribed dot denote differentiation with respect to time t. The dynamics of an n-link robot manipulator are governed by the following equations of motion

$$M\big(q\big)\ddot{q} + V_m\big(q,\dot{q}\big)\dot{q} + G\big(q\big) + F\big(\dot{q}\big) + D = u_T, \tag{1}$$

where the n generalized coordinates contained in the column vector q describe relative joint angles, the square matrix $V_m\big(q,\dot{q}\big)$ contains Coriolis and centripetal effects, the column vector $G\big(q\big)$ represents the effects of gravity and other conservative forces, the column vector $F\big(\dot{q}\big)$ represents dissipative, velocity-dependent mechanisms, for example associated with friction, and the column vectors u_T and D are the time-dependent control input torque and bounded unknown disturbances, respectively. The inertia matrix $M\big(q\big)$ is assumed to be positive-definite, symmetric, and bounded, i.e., such that $\mu_1\mathbb{I} \leq M\big(q\big) \leq \mu_2\mathbb{I}$, for all q and for some positive scalars μ_1 and μ_2, where $\mathbb{I}$ denotes the identity matrix.

Inspired by the sliding control formulation in [5], we introduce the new variable

$$r = (\dot{q} - \dot{q}_d) + \Lambda(q - q_d), \tag{2}$$

where q_d represents desired trajectories for the joint angles and Λ is a symmetric, positive-definite matrix of design parameters, so that (2) is a stable system. This means that as long as the controller maintains a bounded $r(t)$, the joint trajectories $q(t)$ can be solved for in terms of $r(t)$ and are also bounded. In addition, since $-\Lambda$ is Hurwitz, (2) is finite-gain $\mathcal{L}$-stable (see [41]). Therefore, from Lemma A.7.1 in [42], we have

$$\begin{aligned} q(s) &= (s\mathbb{I} + \Lambda)^{-1}r(s) + q_d(s) + (s\mathbb{I} + \Lambda)^{-1}\big(q(0) - q_d(0)\big) \\ \Rightarrow \|q_t\|_{\mathcal{L}_\infty} &\leq \|(s\mathbb{I} + \Lambda)^{-1}\|_{\mathcal{L}_1}\|r_t\|_{\mathcal{L}_\infty} + \|q_d(s) + (s\mathbb{I} + \Lambda)^{-1}\big(q(0) - q_d(0)\big)\|_{\mathcal{L}_\infty}, \end{aligned} \tag{3}$$

where the subscript $_t$ restricts attention to the time interval $[0, t]$. Because $(s\mathbb{I} + \Lambda)^{-1}$ is a proper and stable transfer function, $\|(s\mathbb{I} + \Lambda)^{-1}\|_{\mathcal{L}_1}$ and $\|q_d(s) + (s\mathbb{I} + \Lambda)^{-1}\big(q(0) - q_d(0)\big)\|_{\mathcal{L}_\infty}$ exist and are bounded by positive numbers Q_1 and Q_2 respectively. In other words,

$$\|q_t\|_{\mathcal{L}_\infty} \leq Q_1\|r_t\|_{\mathcal{L}_\infty} + Q_2. \tag{4}$$

Consider the decomposition

$$u_T(t) = u(t) + A_m r(t) \tag{5}$$

of the control input in terms of an adaptive control input $u(t)$ and a Hurwitz matrix A_m that is introduced to shape the transient response of the system dynamics. Substitution of (1) and (5) into the time derivative of (2) then yields

$$\dot{r}(t) = A_m r(t) + u(t) - f\big(t, \zeta(t)\big), \quad r(0) = r_0, \tag{6}$$

where $\zeta^T = \big[r^T, q^T\big]$ and $f\big(t, \zeta(t)\big)$ lumps all the unknown nonlinearities and disturbances.

In the next section, an adaptive controller is designed to estimate this unknown nonlinear function in every computation loop, as well as to control the manipulator to accurately track certain prescribed joint trajectories.

3 A robust adaptive controller

This section develops the control scheme for controlling the robot dynamics presented in the form of (6), the detailed knowledge of the robot model is unknown. The control architecture is depicted in Figure 1 (cf. [42]). Here, the controller's objective is to drive the state r to the desired state $r_d = 0$. The variable $\hat{r}$ represents a *predictor* for r. Similarly, the variables $\hat{\theta}$ and $\hat{\sigma}$ denote *adaptive estimates* for two unknown quantities θ and σ, introduced below.

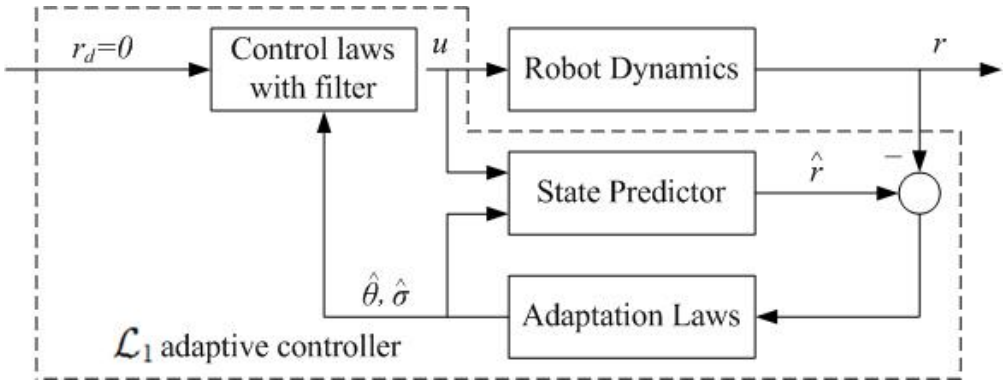

Figure 1: Block diagram of the proposed control system for the manipulator dynamics.

3.1 Parameterization of the nonlinear robot function

Let the unknown nonlinear robot function $f(t, \zeta) : \mathbb{R} \times \mathbb{R}^{2n} \to \mathbb{R}^n$ satisfy the following assumptions:

- There exists a constant $Z > 0$ such that $\|f(t, 0)\|_\infty \leq Z$ for all $t \geq 0$.
- The nonlinear function $f(t, \zeta)$ is continuous in its arguments. For arbitrary δ, there exist $d_{f_t}(\delta) > 0$ and $d_{f_\zeta}(\delta) > 0$ independent of time, such that for all $\|\zeta\|_\infty \leq \delta$, the partial derivatives of $f(t, \zeta)$ with respect to t and ζ are piecewise continuous and bounded:

$$\left\| \frac{\partial f(t,\zeta)}{\partial t} \right\|_\infty \leq d_{f_t}(\delta); \qquad \left\| \frac{\partial f(t,\zeta)}{\partial \zeta} \right\|_\infty \leq d_{f_\zeta}(\delta). \tag{7}$$

Now suppose that $r(t)$ is continuous and (piecewise)-differentiable for all $t \geq 0$, and that $\|r_\tau\|_{\mathcal{L}_\infty} \leq \rho$ and $\|\dot{r}_\tau\|_{\mathcal{L}_\infty} \leq d_r$, for a given $\tau \geq 0$ and in terms of some positive constants ρ and d_r. Finally, let

$$\bar{\rho}(\rho) \triangleq \max\{\rho + \gamma, Q_1(\rho + \gamma) + Q_2\}, \qquad L_\rho \triangleq \frac{\bar{\rho}(\rho)}{\rho} d_{f_\zeta}\big(\bar{\rho}(\rho)\big) \tag{8}$$

for some arbitrary $\gamma > 0$. It follows that $\rho < \bar{\rho}(\rho)$ and, consequently, $d_{f_\zeta}\big(\bar{\rho}(\rho)\big) < L_\rho$. Taking (4) into account, it follows from Lemma A.9.2 in [42] that there exist differentiable functions $\theta(t) \in \mathbb{R}^n$ and $\sigma(t) \in \mathbb{R}^n$ such that the nonlinear function $f\big(t, \zeta(t)\big)$ can be parameterized in $\theta(t)$ and $\sigma(t)$ using $\|r_t\|_{\mathcal{L}_\infty}$ as a regressor:

$$f\big(t, \zeta(t)\big) = \theta(t)\|r_t\|_{\mathcal{L}_\infty} + \sigma(t), \qquad \forall t \in [0, \tau]. \tag{9}$$

In particular, for $t \in [0, \tau]$, the functions θ and σ and their first derivatives are bounded:

$$||\theta(t)||_\infty < \theta_b \qquad ||\dot{\theta}(t)||_\infty < d_\theta \qquad ||\sigma(t)||_\infty < \sigma_b \qquad ||\dot{\sigma}(t)||_\infty < d_\sigma. \tag{10}$$

where $\theta_b \triangleq L_\rho$, $\sigma_b \triangleq L_\rho Q_2 + Z + \epsilon$, in which ϵ is an arbitrary positive constant and d_θ and d_σ are computable bounds.

For $t \in [0, \tau]$, it follows that (6) can be written in the following form:

$$\dot{r}(t) = A_m r(t) + u(t) - \big(\theta(t)\|r_t\|_{\mathcal{L}_\infty} + \sigma(t)\big), \quad r(0) = r_0. \tag{11}$$

3.2 State Predictor

A predictor $\hat{r}$ for the state r is now constructed as follows:

$$\dot{\hat{r}}(t) \;\; = \;\; A_m \hat{r}(t) + u(t) - \big(\hat{\theta}(t)\|r_t\|_{\mathcal{L}_\infty} + \hat{\sigma}(t)\big) - K_{sp}\tilde{r}(t), \quad \hat{r}(0) = r_0, \tag{12}$$

where the *prediction error* $\tilde{r}(t) \triangleq \hat{r}(t) - r(t)$, and K_{sp} is a matrix of loop-shaping parameters that is tuned to reject oscillations caused by high-frequency disturbances or noise.

3.3 Adaptation Laws

Let the adaptive estimates $\hat{\theta}(t)$ and $\hat{\sigma}(t)$ in (12) be governed by the following projection-based laws (cf. [43]):

$$\dot{\hat{\theta}}(t) \;\; = \;\; \Gamma \mathbf{Proj}(\hat{\theta}(t), P\tilde{r}\|r_t\|_{\mathcal{L}_\infty}), \; \hat{\theta}(0) = \hat{\theta}_0, \tag{13}$$

$$\dot{\hat{\sigma}}(t) \;\; = \;\; \Gamma \mathbf{Proj}(\hat{\sigma}(t), P\tilde{r}), \quad \hat{\sigma}(0) = \hat{\sigma}_0. \tag{14}$$

Here, $\Gamma \in \mathbb{R}^+$ is the *adaptation gain* and the matrix $P = P^T > 0$ is the solution to the Lyapunov equation $A_m^T P + P A_m = -Q$, for some arbitrary $Q = Q^T > 0$. The *projection operator* $\mathbf{Proj}(\cdot, \cdot)$ ensures that $\|\hat{\theta}(t)\|_\infty \leq \theta_b$ and $\|\hat{\sigma}(t)\|_\infty \leq \sigma_b$ provided that $\hat{\theta}_0$ and $\hat{\sigma}_0$ satisfy the same bounds. In each of the simulations in Secs. 4 and 5, $\hat{\theta}_0 = \hat{\sigma}_0 = 0$.

3.4 Control Law

Next, let the adaptive control torque in (11) be obtained from the output of the following system

$$u(s) = C(s)\hat{\eta}(s), \tag{15}$$

where $\hat{\eta}(s)$ is the Laplace transform of $\hat{\eta}(t) \triangleq \hat{\theta}(t)\|r_t\|_{\mathcal{L}_\infty} + \hat{\sigma}(t)$. Here, $C(s)$ is a diagonal matrix of BIBO-stable and strictly proper transfer functions with DC gain $C(0) = 1$, assuming zero initialization for its state-space realization. This filter structure decouples the estimation loop from the control loop and allows for arbitrarily large values of the adaptation gain (limited only by available hardware), without hurting the system's robustness.

3.5 Error dynamics

From the previous definitions, the prediction error dynamics are now governed by

$$\dot{\tilde{r}}(t) = (A_m - K_{sp})\tilde{r}(t) - \big(\tilde{\theta}(t)\|r_t\|_{\mathcal{L}_\infty} + \tilde{\sigma}(t)\big), \;\; \tilde{r}(0) = 0, \tag{16}$$

where the *estimation errors* $\tilde{\theta}(t) = \hat{\theta}(t) - \theta(t)$, and $\tilde{\sigma}(t) = \hat{\sigma}(t) - \sigma(t)$ (note that the initial condition r_0 of $r(t)$ and $\hat{r}(t)$ is assumed to be known). One of the objectives of the control design is now to choose A_m, K_{sp}, Γ, Q and the matrix of filters $C(s)$ in order to achieve desirable performance bounds on the error $\tilde{r}$. In the numerical analysis in the next section, we always set $Q = \mathbb{I}$.

3.6 Reference system

In order to obtain design criteria in terms of bounds on the predictability of the state and control input, we construct the closed-loop reference system:

$$\begin{aligned} \dot{q}_{ref}(t) &= \dot{q}_d(t) + r_{ref}(t) - \Lambda\left(q_{ref}(t) - q_d(t)\right), \;\; q_{ref}(0) = q_0 && (17)\\ \dot{r}_{ref}(t) &= A_m r_{ref}(t) + u_{ref}(t) - f(t, \zeta_{ref}(t)), \;\; r_{ref}(0) = r_0, && (18)\\ u_{ref}(s) &= C(s)\eta_{ref}(s), && (19) \end{aligned}$$

where $\zeta_{ref}^T = [r_{ref}^T, q_{ref}^T]$, and $\eta_{ref}(s)$ is the Laplace transform of the signal $\eta_{ref}(t) \triangleq f(t, \zeta_{ref}(t))$.

We sketch the proof of the following theorem in Appendix A.

Theorem 1 *Let ρ_{ref} denote a positive number, chosen such that*

$$\rho_{ref} > \|H(s)r_0\|_{\mathcal{L}_\infty}. \tag{20}$$

Suppose that $\|r_0\|_\infty < \rho_{ref}$ and that $C(s)$ is chosen such that the following condition holds:

$$\|H(s)\big(C(s) - \mathbb{I}\big)\|_{\mathcal{L}_1} < \frac{\rho_{ref} - \|H(s)r_0\|_{\mathcal{L}_\infty}}{L_{\rho_{ref}}\rho_{ref} + Z}, \tag{21}$$

where $L_{\rho_{ref}}$ and Z were introduced in the characterization of the nonlinear robot function f. The state of the reference system is then bounded for all time:

$$\|r_{ref}\|_{\mathcal{L}_\infty} < \rho_{ref}. \tag{22}$$

Moreover,

$$\|u_{ref}\|_{\mathcal{L}_\infty} < \|C(s)\|_{\mathcal{L}_1}\big(L_{\rho_{ref}}\rho_{ref} + Z\big) \triangleq \rho_{u,ref}. \tag{23}$$

3.7 Performance bounds

Suppose that the conditions of Theorem 1 are satisfied by the value of ρ_{ref}, the matrix $C(s)$, and the initial value r_0. We seek to formulate design conditions that guarantee that

$$\begin{aligned} \|\tilde{r}\|_{\mathcal{L}_\infty} &\leq \gamma_0 && (24)\\ \|r_{ref} - r\|_{\mathcal{L}_\infty} &\leq \gamma_1, && (25)\\ \|u_{ref} - u\|_{\mathcal{L}_\infty} &\leq \gamma_2, && (26) \end{aligned}$$

for suitably defined bounds γ_0, γ_1, and γ_2. We sketch the proof of the following theorem in Appendix B.

Theorem 2 *Let γ^* denote the value of γ used in the definition of $\bar{\rho}_{ref}$ (ρ_{ref}) and suppose that γ_0 and β are chosen such that*

$$\gamma_1 \triangleq \frac{\|H(s)C(s)\bar{H}^{-1}(s)\|_{\mathcal{L}_1}}{1 - \|H(s)\big(C(s) - \mathbb{I}\big)\|_{\mathcal{L}_1} L_{\rho_{ref}} Q_m}\gamma_0 + \beta < \gamma^*, \tag{27}$$

where $Q_m \triangleq \max\{1, Q_1\}$ and $\bar{H}(s) \triangleq (s\mathbb{I} - A_m + K_{sp})^{-1}$. Moreover, let

$$\gamma_2 \triangleq \|C(s)\|_{\mathcal{L}_1} L_{\rho_{ref}} Q_m \gamma_1 + \|C(s)\bar{H}^{-1}(s)\|_{\mathcal{L}_1}\gamma_0. \tag{28}$$

The bounds (24)-(26) *then hold, provided that the adaptive gain Γ satisfies the design constraint*

$$\Gamma \geq \frac{\theta_m}{\lambda_{min}(P)\gamma_0^2}, \tag{29}$$

in terms of a computable coefficient θ_m.

We note that one can achieve arbitrarily small performance bounds γ_0, γ_1 and γ_2 by increasing the adaptive gain Γ.

3.8 Simulation model

We restrict attention in the remainder of this paper to a typical pick-and-place manipulator, as shown in Fig. 2, in which q_1, q_2, and q_3 are the relative joint angles between the homogeneous links and (x_b, y_b, z_b) represents the time-dependent position of the manipulator base, treated as an unknown disturbance in the analysis below. Here, gravity is assumed to act along the negative z-axis. In the numerical results reported below, and in a set of consistent units (the SI system is used throughout the paper), the link lengths, the masses of the three links, the payload at the end-effector, and the acceleration of gravity are given by $L_1 = 0.25;\ L_2 = 0.2;\ L_3 = 0.1;\ m_1 = 1.25;\ m_2 = 1;\ m_3 = 0.25;\ m_e = 1.25;\ g = 9.81.$

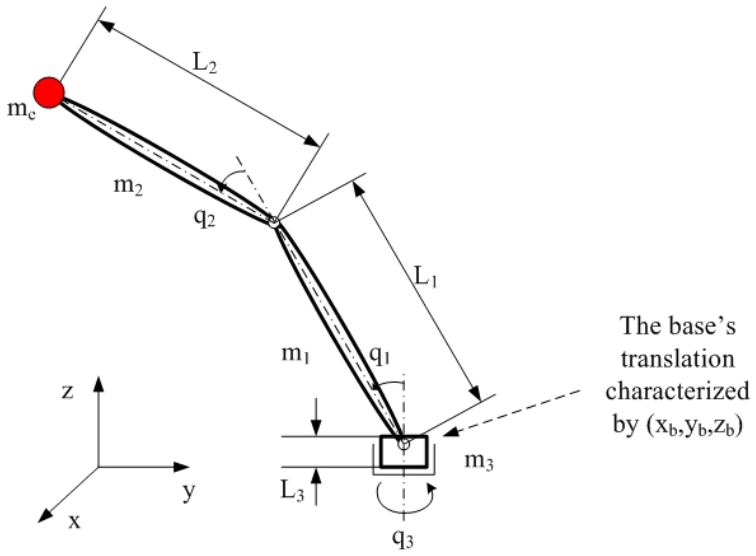

Figure 2: Typical pick-and-place manipulator with moving base.

4 Trajectory tracking

We begin by illustrating the performance of the control design when the joint angles are tasked to track predefined

- step reference inputs with $q_{1,d}(t) = q_{2,d}(t) = q_{3,d}(t) \equiv \alpha$, for values of $\alpha \in [0, 2]$, with $q_0 = \dot{q}_0 = (0, 0, 0)^T$ and
- sinusoidal reference inputs with $q_{1,d}(t) = q_{2,d}(t) = \sin \frac{2}{3}t$ and $q_{3,d}(t) = \cos \frac{2}{3}t$ with $q_0 = (0, 0, 1)^T$ and $\dot{q}_0 = (0, 0, 0)^T$.

In the simulations in this paper, the control parameters and the filter are tuned to the following control objectives:

- In the case of the step reference inputs, achieve a response settling time (the time required for the response to reach and stay within 2% of the final value) of less than 5 s, with zero overshoot.
- In the case of the sinusoidal reference inputs, achieve a root-mean-square (RMS) tracking error of less than 0.07 under various disturbances including time delay, base motion, and measurement noise.

To this end, the filter matrix in (2) is here set to equal $\Lambda = \mathbb{I}$, the adaptive gain Γ is set to 10^5, and the transient response characteristics are governed by the design matrix $A_m = -5\mathbb{I}$. A second-order filter $C(s) = \omega_c^2/(s^2 + 2\xi\omega_c s + \omega_c^2)$ with bandwidth of $\omega_c = 12$ and damping factor of $\xi = 0.7$ is employed. We rely on the result in [44] to set the matrix of loop-shaping parameters K_{sp} in the state-predictor design (12) to $6\sqrt{\Gamma}\mathbb{I} + A_m$.

The numerical results below were obtained from a Simulink-based implementation of the manipulator equations of motion and the $\mathcal{L}_1$ control architecture, described above. Default Simulink tolerances and settings were used throughout.

4.1 Performance in ideal working conditions

Figure 3 and 4 show the response of the manipulator to the $\mathcal{L}_1$ control actuation in the case of step reference inputs with different values of α and the sinusoidal reference input, respectively. As seen in the bottom panels, for both types of reference inputs, the $\mathcal{L}_1$ control signals are smooth and clean, in spite of the use of high-rate estimation to accommodate nonlinearity and model uncertainty while retaining small prediction errors. For the step reference input, no overshoot is observed, and the maximum settling time is 4.45 s. As seen in Figure 3, the system response scales approximately uniformly with the size of the step reference input. For the sinusoidal reference input, the maximum RMS tracking error is 0.0589.

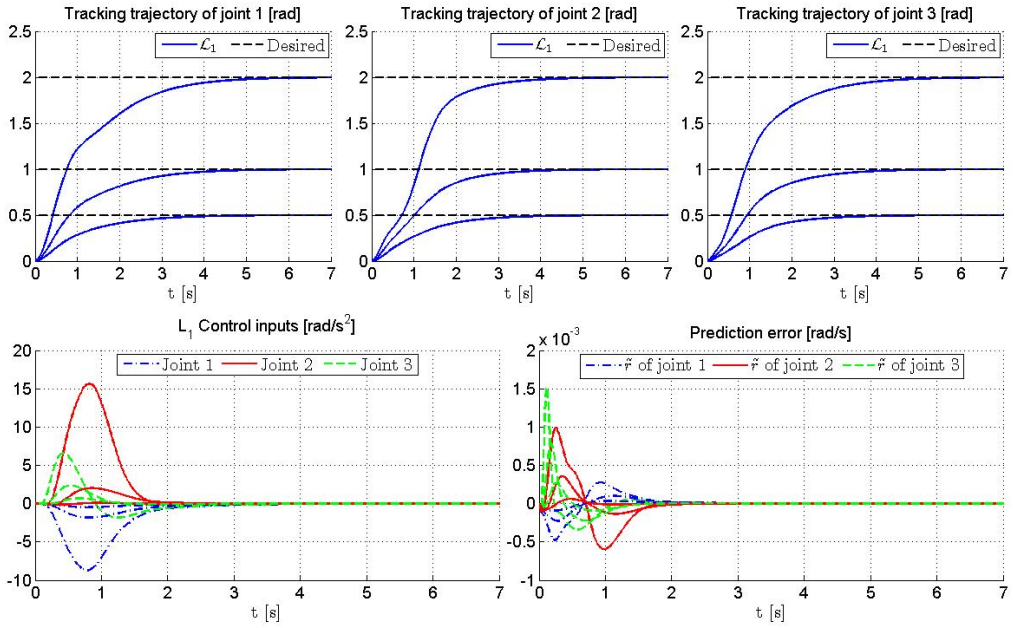

Figure 3: Performance of the proposed controller in ideal working conditions with various step reference inputs: The top row shows the actual joint angles $q(t)$ (solid) together with the desired joint trajectories $q_d(t)$ (dashed) as a function of time t. The bottom row displays the components of the control input $u(t)$ and the prediction error $\tilde{r}(t)$.

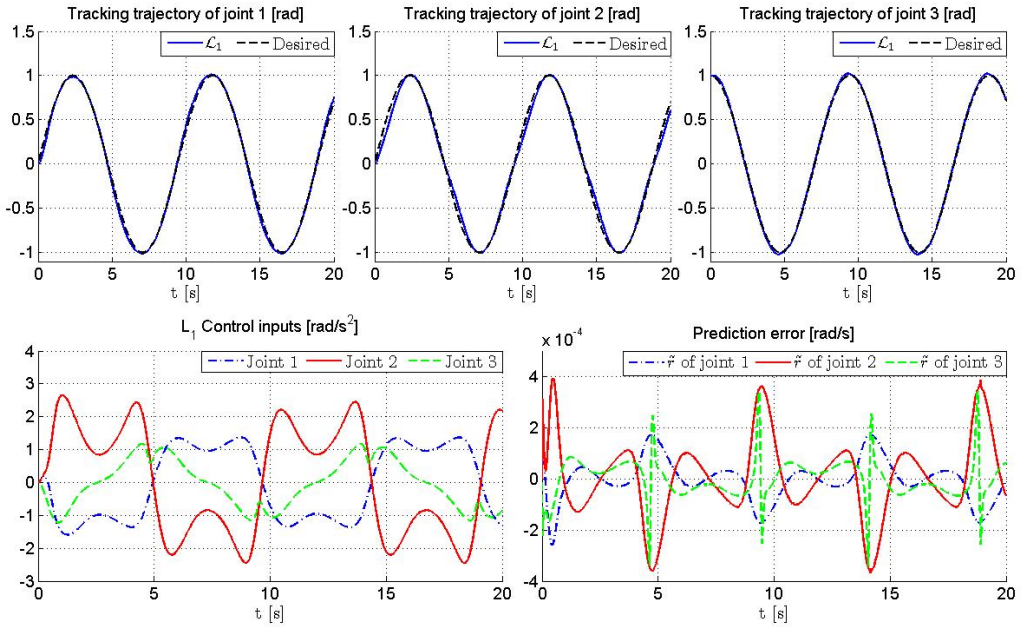

Figure 4: Performance of the proposed controller in ideal working conditions with sinusoidal reference inputs: The top row shows the actual joint angles $q(t)$ (solid) together with the desired joint trajectories $q_d(t)$ (dashed). The bottom row displays the components of the control input $u(t)$ and the prediction error $\tilde{r}(t)$.

4.2 Robustness

We proceed to analyze the robustness of the $\mathcal{L}_1$ control system by investigating its performance in the presence of time delays at the plant input. Specifically, we define the *critical time delay* as the maximum actuator time delay, for which the controller is able to maintain bounded performance, for a given choice of system parameters and desired trajectory $q_d(t)$.

For the current set of parameters and the sinusoidal input reference, with a time delay of 150 ms or less, the controller gives almost the same performance as that obtained without delay in Fig. 4. When a time delay of 180 ms is introduced in the system, the tracking performance of the proposed controller remains desirable, as illustrated in Fig. 5 with a maximum RMS tracking error of 0.0675. For this time delay, however, oscillations begin to appear in the control signals. These oscillations can be largely eliminated by introducing a time delay in the state predictor (see [45]). Such a systematic modification to the state predictor by incorporating known delays hence improves the system robustness. As the actuator time delay is increased further, the system performance deteriorates gradually, and an unbounded response is obtained for a delay of 233 ms. In the $\mathcal{L}_1$ control architecture, it is possible to improve the critical time delay by suitable tuning of the filter $C(s)$. For instance, with a filter bandwidth of 8 and the same damping factor of 0.7, the critical time delay is increased to 275 ms.

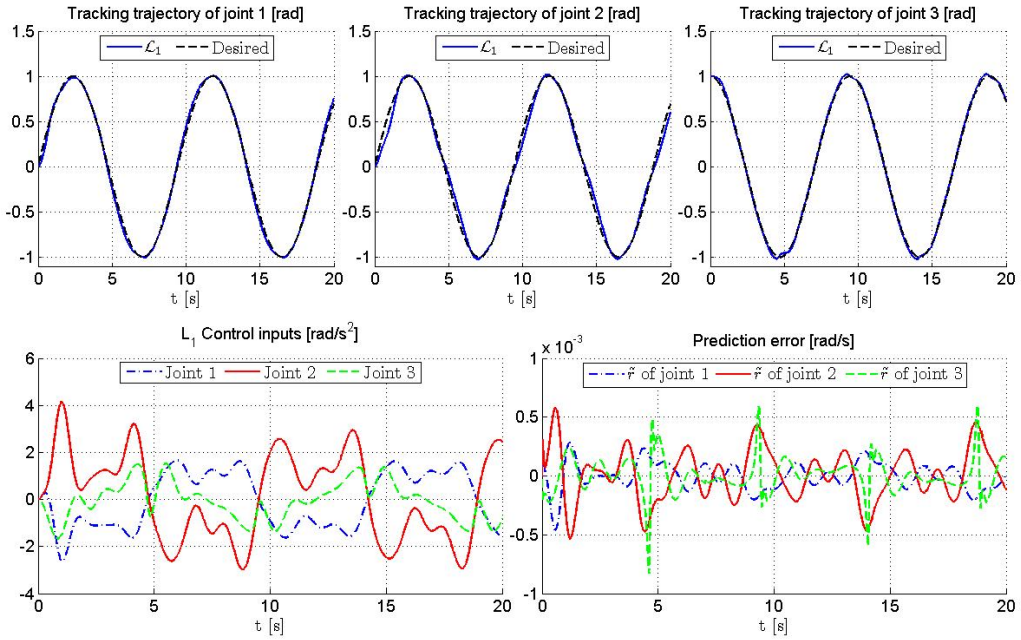

Figure 5: Performance of the proposed controller with actuator time delay of 180 ms without re-tuning: The top row shows the actual joint angles $q(t)$ (solid) together with the desired joint trajectories $q_d(t)$ (dashed). The bottom row displays the components of the control input $u(t)$ and the prediction error $\tilde{r}(t)$.

4.3 Control performance under base motion

We consider next the response of the control system to base motion acceleration of the form

$$\begin{cases} \ddot{x}_b = 0.8 \sin 20t, \\ \ddot{y}_b = 0.8 \cos 20t, \\ \ddot{z}_b = 0.8 \cos 20t. \end{cases} \tag{30}$$

The desired trajectories and initial conditions remain unchanged as in the previous sections. The unknown base movement in (30) can be thought of as unmodeled dynamics or a disturbance. As shown in Fig. 6, there is minimal effect on the tracking performance of the controller with the maximum RMS tracking error of 0.0605. Although the control signal contains the additional frequency component associated with the base acceleration, it remains smooth and implementable.

4.4 Control performance with measurement noise

Finally, we consider the performance of the control system in the presence of velocity measurement noise. To this end, unfiltered, uniformly distributed noise in the range $[-0.1, 0.1]$ rad/s and with sample time of 0.01 s was added to the angular velocity measurements. As seen in Fig. 7, without any further tuning, the proposed controller successfully rejects the noise. The control scheme still maintains desirable tracking performance with the maximum RMS tracking error of 0.0599. In addition, the control signals are relatively clean and implementable.

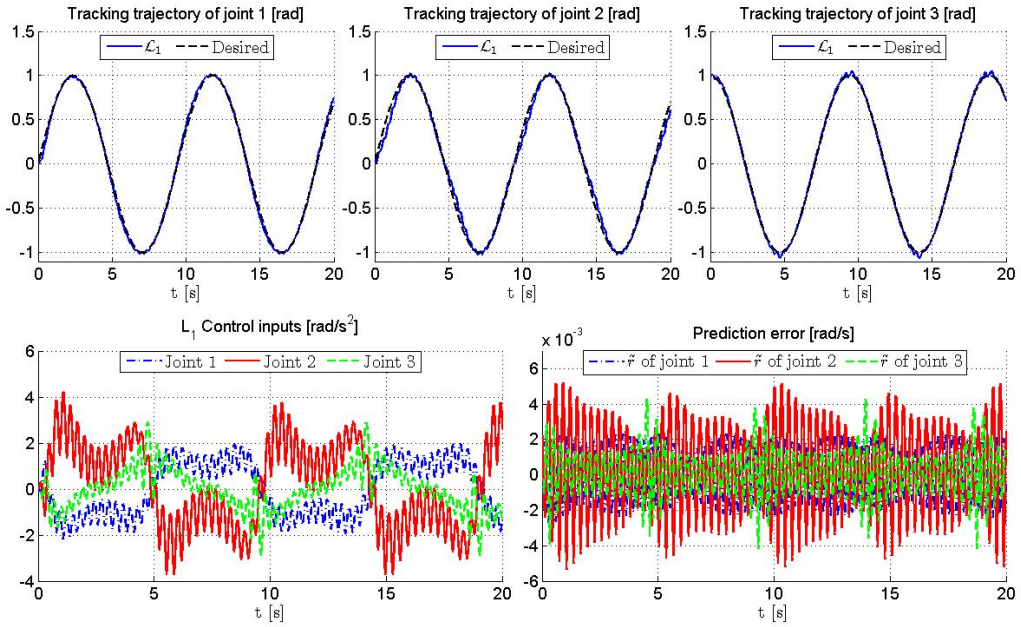

Figure 6: Performance of the proposed controller with base motion: The top row shows the actual joint angles $q(t)$ (solid) together with the desired joint trajectories $q_d(t)$ (dashed). The bottom row displays the components of the control input $u(t)$ and the prediction error $\tilde{r}(t)$.

5 Command Following and Switching

We consider next the application of the $\mathcal{L}_1$ control design to a command-following task, in which the motion of the manipulator end-effector tracks an unknown desired trajectory through observations of the deviation between the actual and the desired position. This models the situation in which the end-effector of the manipulator interacts with a user's wrist via force sensors, and follows the wrist movement by minimizing any interaction forces.

We assume below that the interaction force is given by

$$F_{hm} = \begin{pmatrix} F_x \\ F_y \\ F_z \end{pmatrix} := k_s \begin{pmatrix} x_d - x \\ y_d - y \\ z_d - z \end{pmatrix}, \tag{31}$$

where k_s is the effective stiffness of the force sensor; $[x \;\; y \;\; z]^T$ is the current position of the end-effector, which can be calculated by the following forward kinematics:

$$\begin{aligned} x &= \big(L_1 s_1 + L_2 s_{1+2}\big) c_3, \\ y &= \big(L_1 s_1 + L_2 s_{1+2}\big) s_3, \\ z &= L_1 c_1 + L_2 c_{1+2}; \end{aligned} \tag{32}$$

and $[x_d \;\; y_d \;\; z_d]^T$ are the unknown coordinates of the desired position of the end-effector. Here and below, s_1 refers to $\sin q_1$ and s_{1+2} to $\sin(q_1 + q_2)$ and similarly for other index values and the cosine function. In this case, the manipulator equations of motion in (6) become:

$$\dot{r}(t) = A_m r(t) + u(t) - f\big(t, \zeta(t)\big) + M^{-1}\big(q(t)\big) T_{hm}, \quad r(0) = r_0, \tag{33}$$

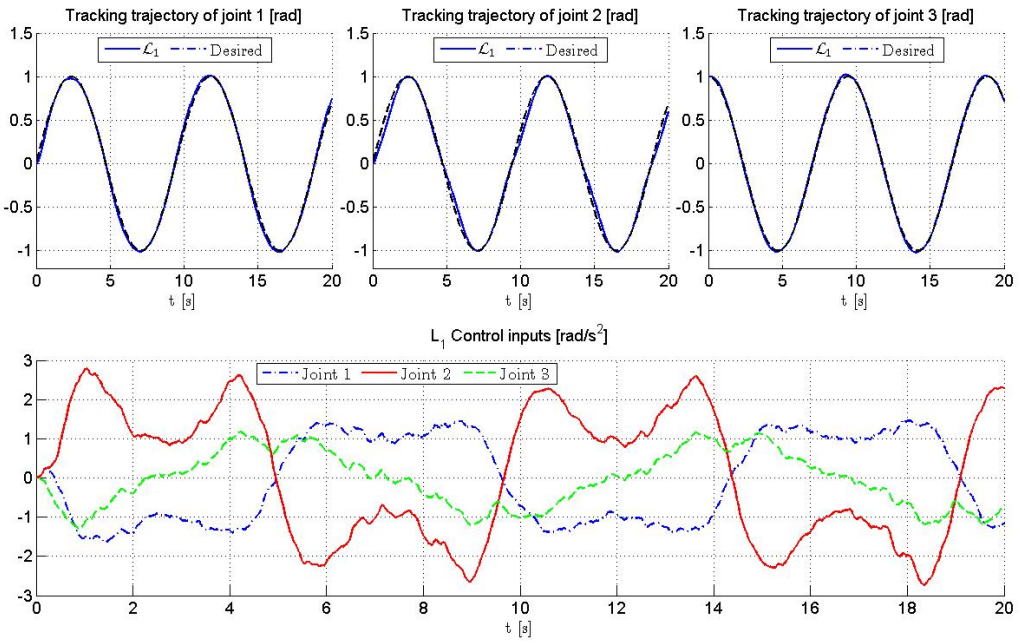

Figure 7: Performance of the proposed controller in the presence of velocity measurement noise in the range $[-0.1,\ 0.1]$ rad/s and with sample time of 0.01 s: The top row shows the actual joint angles $q(t)$ (solid) together with the desired joint trajectories $q_d(t)$ (dashed). The bottom row displays the components of the control input $u(t)$.

where T_{hm} represents a column vector of generalized forces that can be obtained from F_{hm} as follows:

$$T_{hm} = \begin{pmatrix} (L_1c_1 + L_2c_{1+2})c_3 & (L_1c_1 + L_2c_{1+2})s_3 & -(L_1s_1 + L_2s_{1+2}) \\ L_2c_{1+2}c_3 & L_2c_{1+2}s_3 & -L_2s_{1+2} \\ -(L_1s_1 + L_2s_{1+2})s_3 & (L_1s_1 + L_2s_{1+2})c_3 & 0 \end{pmatrix} F_{hm}. \tag{34}$$

The same control architecture with predictor dynamics (12), adaptation laws (13) and (14), and control input (15) are used to control this system. Here, we construct a reference trajectory on the fly, by requiring that q_d satisfy the following constitutive relation

$$\dot{q}_d \frac{\partial h}{\partial q_d}(q_d, t) + \frac{\partial h}{\partial t}(q_d, t) + \Psi h(q_d, t) = 0, \quad q_d(0) = q_0, \tag{35}$$

where Ψ is a diagonal matrix of positive constants;

$$h(q_d, t) \triangleq \begin{pmatrix} (L_1 \sin q_{d1} + L_2 \sin(q_{d1} + q_{d2})) \cos q_{d3} - x_d(t) \\ (L_1 \sin q_{d1} + L_2 \sin(q_{d1} + q_{d2})) \sin q_{d3} - y_d(t) \\ L_1 \cos q_{d1} + L_2 \cos(q_{d1} + q_{d2}) - z_d(t) \end{pmatrix}; \tag{36}$$

and $x_d(t)$, $y_d(t)$, $z_d(t)$, and their time derivatives are obtained from (31) using filtered measurements of the interaction force and forward kinematics of the measured joint angles.

Now let static positioning be defined as a special case of trajectory tracking in which the predefined desired joint motions are constant and equal to the actual joint angles at the onset of tracking. We consider below a strategy for switching between static positioning and command following, in which $q_d(t)$ is continuous everywhere except at moments corresponding to a switch to static positioning. It follows that at such a moment, the initial condition r_0 must be set to equal the value of $\dot{q}$.

Let F_{cr} and V_{cr} denote preset critical values of the magnitude of the interaction force and the speed of the manipulator end-effector, respectively. We associate the case of static positioning to a phase during which the magnitude of the measured interaction force is less than F_{cr} and the measured speed of the manipulator end-effector is less than V_{cr}. Similarly, we associate the case of command following to a phase during which either the measured interaction force exceeds F_{cr} or the measured end-effector speed exceeds V_{cr}. A switch from static positioning to command following then occurs when either the force or the velocity exceed the corresponding critical value. Similarly, a switch from command following to static positioning occurs when both the force and velocity fall below the corresponding critical values. In practice the interaction force will exceed F_{cr} before the end-effector speed exceeds V_{cr}, given a phase of static positioning.

To simulate a practical scenario, the manipulator is initialized by following step reference inputs from a resting configuration to a desired position. After the manipulator stabilizes around the desired position at $t = 5$, the control algorithm is switched to a phase of static positioning, during which a user starts interacting with the manipulator's end-effector and interaction forces are measured. At $t = 6.5$, the user's wrist starts moving. The controller uses the proposed strategies to decide when to switch to command following. Here, we let $F_{cr} = 0.05$ and $V_{cr} = 0.05$. The former is equivalent to an effective displacement of 0.01 between the position of the human wrist and that of the manipulator's end-effector, given a sensor stiffness of $k_s = 5$. The desired path is equivalent to the following time histories (cf. Fig. 9).

$$\begin{aligned} x_d(t) &= 0.0625 + 0.05\cos(t), \\ y_d(t) &= 0.125 + 0.0625\sin(t), \\ z_d(t) &= 0.0125t, \end{aligned} \tag{37}$$

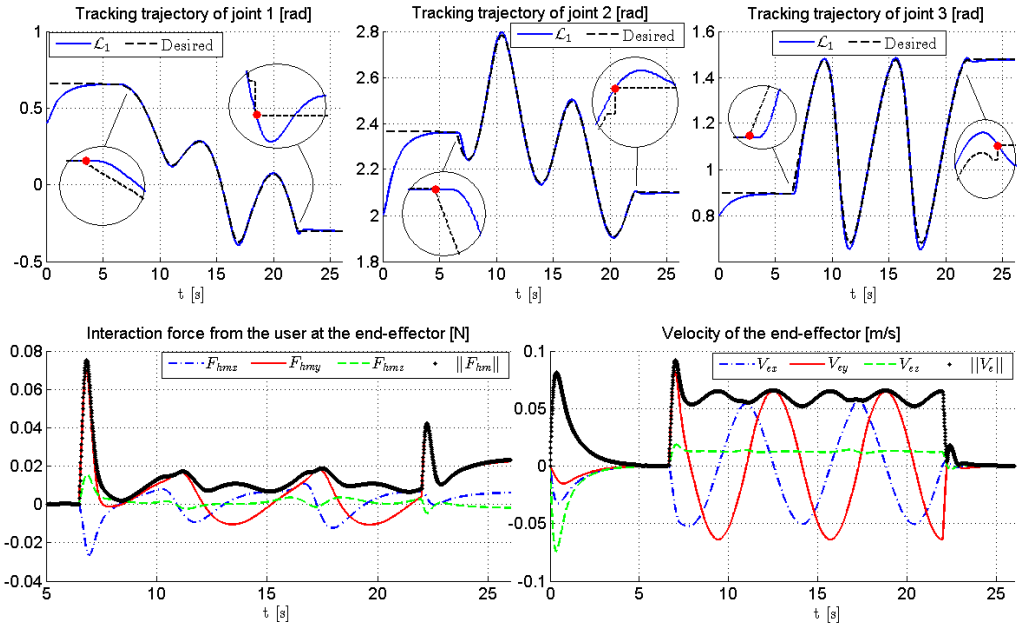

Figure 8: Performance of the switching task: The top row shows the actual joint angles $q(t)$ (solid) together with the desired joint trajectories $q_d(t)$ (dashed) with zoomed-in figures of the switching interval. The filled circles in each of these figure indicate the onset and termination of wrist motion, in each case followed by the controller switching from static positioning to command following, and vice versa. The panels in the bottom row display the components and magnitude of the measured interaction force and magnitude and the measured velocity of the end-effector, respectively.

As stated previously, the desired path is not known a priori to the controller. Instead, the locus of the user's wrist is estimated in every loop based on the joint angle and force measurements. In the numerical results, these measurements are filtered through a first-order filter with bandwidth 100 prior to further processing (e.g., differentiation). In the $\mathcal{L}_1$ controller, the same control parameters and filter $C(s)$ as in the previous sections are employed. The diagonal matrix Ψ in (35) is set equal to $5\mathbb{I}$. At $t = 22$, the user stops moving, and the controller switches back to static positioning when both the interaction force and the end-effector's speed fall below the corresponding critical values. Figure 8 shows the performance of the $\mathcal{L}_1$ control strategy, using the parameter values given in Sec. 4, combined with the switching strategy described above, in the absence of measurement noise and base motion, but with model uncertainty and nonlinearity. The top row shows the joint trajectories vs. the desired trajectories; the bottom row shows the interaction force and the end-effector speed. Initialization occurs during the first five seconds. The manipulator's resting configuration is assumed to be $q = (0.4,\ 2,\ 0.8)^T$. Static positioning of the end-effector begins at $t = 5$ and is maintained until the measured interaction force exceeds the critical value following the onset of wrist motion at $t = 6.5$. The controller then switches to the command-following strategy, where the desired path is inferred from the interaction force measurements, in order to follow the desired path of the user's wrist. When the speed of the manipulator end-effector and the interaction force both fall below the corresponding critical values, the controller switches back to the static positioning control scheme (in the last four seconds). It is observed that at the onset of static positioning, q_d exhibits a jump discontinuity, such that q_d equals the actual joint angles following the jump. Figure 9 illustrates the end-effector's path and the desired path of

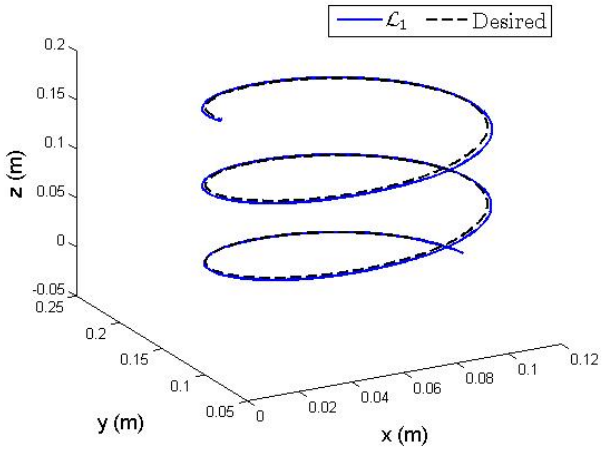

Figure 9: End-effector path in physical space during the control task described in Sec. 5 using the proposed control architecture and the switching scheme between command following and static positioning.

the user's wrist in space. After the initial phase of static positioning, the manipulator end-effector's path $[x \;\; y \;\; z]^T$ quickly settles to a smooth curve that closely follows the desired path $[x_d \;\; y_d \;\; z_d]^T$. The maximal F_{hm} experienced during the command-following task clearly depends on the numerical values of the control parameters, as well as the filters' bandwidth.

6 Conclusion

This paper has described a robust adaptive controller based on the $\mathcal{L}_1$ control architecture for robot manipulators. As evidenced by fundamental theoretical results on the existence of computable performance bounds, this framework successfully separates the adaptation loop from the control loop, thereby allowing for arbitrary increases in the adaptation rate (bounded only by hardware constraints) without sacrificing the system's robustness, and allows for a predictable transient response with smooth and implementable control signals. With the introduction of a variable transformation, inspired by earlier work in [5], and an innovative control design, the formulation is able to compensate for the nonlinearity and uncertainties in the dynamic model without the need for the inversion of inertia matrix.

Numerical simulations were used to illustrate the control paradigm in the context of a trajectory tracking task imposed on a three-degree-of-freedom robot arm, for a known reference input, as well as in the case of one inferred on the fly using end-effector measurements and inverse kinematics. The results demonstrate desirable tracking performance and clean and smooth control input with different types of disturbances, including intense base motion, measurement noise, and time delay. A switching strategy between static positioning (constant desired joint angles) and command following (inferred desired joint angles) was also presented and successfully tested. This opens the promising opportunity of $\mathcal{L}_1$ control in robotic applications, where time delay or unmodeled dynamics are unavoidable, for example teleoperation, mobile manipulation, and bioassistive devices.

The successful design of the adaptive control architecture relies upon a key parameterization of the nonlinear contribution to the robot equations of motion in two time-varying parameters with the $\mathcal{L}_\infty$-norm of the state as a regressor. The controller further employs projection operators in the adaptive laws to impose

bounds on the parameter estimates, and uses filters in the control input to keep the control-signal frequencies below the available control-system bandwidth. In this case, Theorem 2 implies close agreement between the system response and the control input, on the one hand, and the corresponding time histories for a suitably formulated reference system, on the other hand, provided that the adaptive gain is chosen sufficiently large. The deviation between the system response and the desired trajectory observed in the numerical results may be traced to the need to maintain a finite filter bandwidth, in order to guarantee robustness. This is the design trade-off between performance and robustness of the proposed control architecture.

We finally comment on the observations made regarding the critical time delay during the two trajectory tracking tasks considered above. As seen in [42] in the linear case, the basic $\mathcal{L}_1$ control architecture supports the formulation of theoretical lower bounds on the time delay margin, through the use of a suitably formulated equivalent LTI system. Some degree of robustness is therefore guaranteed provided that the adaptation gain is sufficiently large. Work is currently underway [45] to adapt these theoretical results to the manipulator context. For static and periodic reference inputs, a systematic analysis of the dependence on the actual critical time delay on the control parameters may be obtained, for example, using techniques of numerical continuation. We will return to these considerations in a future publication.

Acknowledgement

This work was partially supported by AFOSR and a NASA SBIR Phase I contract, order no. NNX12CE97P, awarded to CU Aerospace, L.L.C. We would like to thank Evgeny Kharisov for his support in the simulation of the proposed control algorithm.

A Proof of Theorem 1

The reference system in (18) may be expressed in the Laplace domain in terms of the matrix $H(s) \triangleq (s\mathbb{I} - A_m)^{-1}$ of proper transfer functions:

$$r_{ref}(s) \;\; = \;\; H(s)\big(C(s) - \mathbb{I}\big)\eta_{ref}(s) + H(s)r_0. \tag{38}$$

If (22) is not true, there exists some $\tau > 0$ such that

$$\|r_{ref\,\tau}\|_{\mathcal{L}_\infty} = \rho_{ref}, \tag{39}$$

and, since $\|r_{ref}(0)\|_\infty = \|r_0\|_\infty < \rho_{ref}$,

$$\|r_{ref}(t)\|_\infty < \rho_{ref} \;\; \forall t \in [0, \tau), \;\; \text{and} \;\; \|r_{ref}(\tau)\|_\infty = \rho_{ref}. \tag{40}$$

It follows that

$$\|\zeta_{ref\,\tau}\|_{\mathcal{L}_\infty} \leq \max\{\|r_{ref\,\tau}\|_{\mathcal{L}_\infty}, Q_1\|r_{ref\,\tau}\|_{\mathcal{L}_\infty} + Q_2\} < \bar{\rho}_{ref}(\rho_{ref}), \tag{41}$$

where $\bar{\rho}_{ref}$ is given by (8) in terms of some arbitrary positive constant γ.

The uniform boundedness of the partial derivatives of $f(t, \zeta)$ in assumption (7) now implies that

$$\begin{aligned} \|\big(f(t, \zeta_{ref}) - f(t, 0)\big)_\tau\|_{\mathcal{L}_\infty} \;\; &\leq \;\; d_{f_\zeta}\big(\bar{\rho}_{ref}(\rho_{ref})\big)\|\zeta_{ref\,\tau}\|_{\mathcal{L}_\infty} \\ \Rightarrow \|\eta_{ref\,\tau}\|_{\mathcal{L}_\infty} \;\; &< \;\; L_{\rho_{ref}}\rho_{ref} + Z. \end{aligned} \tag{42}$$

It follows from (38) and Lemma A.7.1 in [42] that

$$\|r_{ref\,\tau}\|_{\mathcal{L}_\infty} \;\leq\; \|H(s)\big(C(s)-\mathbb{I}\big)\|_{\mathcal{L}_1}\|\eta_{ref\,\tau}\|_{\mathcal{L}_\infty} + \|H(s)r_0\|_{\mathcal{L}_\infty}. \tag{43}$$

Substitution of (42) and the stability condition (21) in (43) yields $\|r_{ref\,\tau}\|_{\mathcal{L}_\infty} < \rho_{ref}$, in contradiction to (39).

From (22), it follows that (42) holds for arbitrary τ. The bound in (23) is obtained by applying (42) to the norm inequality of the control input in (19):

$$\|u_{ref}\|_{\mathcal{L}_\infty} \leq \|C(s)\|_{\mathcal{L}_1}\|\eta_{ref}\|_{\mathcal{L}_\infty}. \tag{44}$$

B Proof of Theorem 2

Suppose that the bounds in (25) and (26) are not true. Because $\|r_{ref}(0)-r(0)\| = 0 < \gamma_1$ and $\|u_{ref}(0)-u(0)\| = 0 < \gamma_2$, and since $r_{ref}(t)$, $r(t)$, $u_{ref}(t)$ and $u(t)$ are continuous functions, there exists $\tau > 0$ such that

$$\|r_{ref}(t)-r(t)\|_\infty < \gamma_1, \quad \|u_{ref}(t)-u(t)\|_\infty < \gamma_2, \;\; \forall t \in [0,\tau), \tag{45}$$

and

$$\|r_{ref}(\tau)-r(\tau)\|_\infty = \gamma_1 \text{ or } \|u_{ref}(\tau)-u(\tau)\|_\infty = \gamma_2. \tag{46}$$

This means at least one of the following inequalities is true:

$$\|(r_{ref}-r)_\tau\|_{\mathcal{L}_\infty} = \gamma_1 \text{ or } \|(u_{ref}-u)_\tau\|_{\mathcal{L}_\infty} = \gamma_2. \tag{47}$$

Let

$$\rho^* \;\triangleq\; \rho_{ref} + \gamma^*, \tag{48}$$

$$\rho_u \;\triangleq\; \rho_{u,ref} + \gamma_2. \tag{49}$$

It follows from Theorem 1 that

$$\|r_\tau\|_{\mathcal{L}_\infty} \leq \rho^*, \;\; \|u_\tau\|_{\mathcal{L}_\infty} \leq \rho_u \tag{50}$$

and thus that

$$\begin{aligned} \|\zeta_\tau\|_{\mathcal{L}_\infty} &\leq \max\{\|r_\tau\|_{\mathcal{L}_\infty}, Q_1\|r_\tau\|_{\mathcal{L}_\infty}+Q_2\} \leq \max\{\rho^*, Q_1\rho^*+Q_2\} \\ &= \max\{\rho_{ref}+\gamma^*, Q_1(\rho_{ref}+\gamma^*)+Q_2\} = \bar{\rho}_{ref}\left(\rho_{ref}\right). \end{aligned} \tag{51}$$

By considering the following Lyapunov function candidate

$$V\big(\tilde{r}(t),\tilde{\theta}(t),\tilde{\sigma}(t)\big) = \tilde{r}^T(t)P\tilde{r}(t) + \frac{1}{\Gamma}\big(\tilde{\theta}^2(t)+\tilde{\sigma}^2(t)\big), \tag{52}$$

one can prove in the same way as in [42] that

$$\|\tilde{r}_\tau\| \leq \sqrt{\frac{\theta_m}{\lambda_{min}(P)\Gamma}}, \tag{53}$$

where

$$\theta_m \triangleq 4\theta_b^2 + 4\sigma_b^2 + 4\frac{\lambda_{max}(P)}{\lambda_{min}(Q)}\big(\theta_b d_\theta + \sigma_b d_\sigma\big). \tag{54}$$

Hence, if Γ is selected to satisfy the design constraint in (29), then

$$\|\tilde{r}_\tau\| \leq \gamma_0. \tag{55}$$

It follows from (4) and (17) that

$$\|(q_{ref} - q)_\tau\|_{\mathcal{L}_\infty} \leq Q_1 \|(r_{ref} - r)_\tau\|_{\mathcal{L}_\infty}. \tag{56}$$

Together with (41) and (51), the uniform boundedness of the partial derivatives of $f(t,\zeta)$ in assumption (7) then implies that

$$\begin{aligned} \|(\eta_{ref} - \eta)_\tau\|_{\mathcal{L}_\infty} &\leq d_{f_\zeta}\big(\bar{\rho}_{ref}(\rho_{ref})\big)\|(\zeta_{ref} - \zeta)_\tau\|_{\mathcal{L}_\infty} \\ &\leq L_{\rho_{ref}} Q_m \|(r_{ref} - r)_\tau\|_{\mathcal{L}_\infty}, \end{aligned} \tag{57}$$

where $\eta(t) \triangleq f\left(t, \zeta(t)\right)$. Now let $\bar{H}(s) \triangleq \big(s\mathbb{I} - A_m + K_{sp}\big)^{-1}$. From (6), (16), and (18), we obtain

$$\begin{aligned} r_{ref}(s) - r(s) &= H(s)\big(C(s) - \mathbb{I}\big)\big(\eta_{ref}(s) - \eta(s)\big) + H(s)C(s)\bar{H}^{-1}(s)\tilde{r}(s) \\ \Rightarrow \|(r_{ref} - r)_\tau\|_{\mathcal{L}_\infty} &\leq \|H(s)\big(C(s) - \mathbb{I}\big)\|_{\mathcal{L}_1} L_{\rho_{ref}} Q_m \|(r_{ref} - r)_\tau\|_{\mathcal{L}_\infty} + \|H(s)C(s)\bar{H}^{-1}(s)\|_{\mathcal{L}_1}\gamma_0 \\ \Rightarrow \|(r_{ref} - r)_\tau\|_{\mathcal{L}_\infty} &\leq \frac{\|H(s)C(s)\bar{H}^{-1}(s)\|_{\mathcal{L}_1}}{1 - \|H(s)\big(C(s) - \mathbb{I}\big)\|_{\mathcal{L}_1} L_{\rho_{ref}} Q_m}\gamma_0 = \gamma_1 - \beta < \gamma_1. \end{aligned} \tag{58}$$

Furthermore, it follows from (15) and (19) that

$$\begin{aligned} u_{ref}(s) - u(s) &= C(s)\big(\eta_{ref}(s) - \eta(s)\big) + C(s)\bar{H}^{-1}(s)\tilde{r}(s) \\ \Rightarrow \|(u_{ref} - u)_\tau\|_{\mathcal{L}_\infty} &\leq \|C(s)\|_{\mathcal{L}_1} L_{\rho_{ref}} Q_m(\gamma_1 - \beta) + \|C(s)\bar{H}^{-1}(s)\|_{\mathcal{L}_1}\gamma_0 < \gamma_2 \end{aligned} \tag{59}$$

As the results in (58) and (59) contradict each of the equalities in (47), the bounds in (25) and (26) must follow. Consequently, the bounds in (50) hold uniformly for all time. From here one can use the same Lyapunov function in (52) to prove that the bounds in (53) and (55) hold uniformly for all time provided that Γ is chosen appropriately.

References

[1] Dubowsky S, DesForges DT. The application of model reference adaptive control to robotic manipulators. *Journal of Dynamic Systems, Measurement and Control* 1979; **101**:193-200.

[2] Nicosia S, Tomei P. Model reference adaptive control algorithms for industrial robots. *Automatica* 1984; **20**(5):635-644.

[3] Horowitz R, Tomizuka M. An Adaptive Control Scheme for Mechanical Manipulators - Compensation of Nonlinearity and Decoupling Control. *Journal of Dynamic Systems, Measurement, and Control* 1986; **108**:127-136.

[4] Craig JJ, Hsu P, Sastry SS. Adaptive Control of Mechanical Manipulators. *International Journal of Robotics Research* 1987; **6**(2):16-28.

[5] Slotine JJE, Li W. On the adaptive control of robot manipulators. *International Journal of Robotics Research* 1987; **6**(3):49-59.

[6] Kaneko K, Horowitz R. Repetitive and adaptive control of robot manipulators with velocity estimation. *IEEE Transactions on Robotics and Automation* 1997; **13**(2):204-217

[7] Sirouspour MR, Salcudean SE. Nonlinear control of hydraulic robots. *IEEE Transactions on Robotics and Automation* 2001; **17**(2):173-182.

[8] Cheah CC, Liu C, Slotine, JJE. Adaptive Jacobian tracking control of robots with uncertainties in kinematic, dynamic and actuator models. *IEEE Transactions on Automatic Control* 2006, **51**(6):1024-1029.

[9] Wang H, Liu YH, Zhou D. Adaptive Visual Servoing Using Point and Line Features With an Uncalibrated Eye-in-Hand Camera. *IEEE Transactions on Robotics* 2008; **24**(4):843-857.

[10] Boning P, Dubowsky S. A Kinematic Approach to Determining the Optimal Actuator Sensor Architecture for Space Robots. *The International Journal of Robotics Research* 2011; **30**(9):1194-1204.

[11] Ortega R, Spong MW. Adaptive motion control of rigid robots: A tutorial. *Automatica* 1989; **25**(6):877-888, .

[12] Brogliato B, Landau ID, Lozano-Leal R. Adaptive motion control of robot manipulators: A unified approach based on passivity. *The International Journal Robust and Nonlinear Control* 1991; **1**:187-202.

[13] Niemeyer G, Slotine JJE. Stable adaptive teleoperation. *IEEE Journal of Oceanographic Engineering* 1991; **16**(1):152-162.

[14] Berghuis H, Nijmeijer H. A passivity approach to controller-observer design for robots. *IEEE Transactions on Robotics and Automation* 1993; **9**(6):740-754.

[15] Ortega R and van de Schaft AJ, Maschke B, Escobar G. Interconnection and damping assignment passivity-based control of port-controlled Hamiltonian systems. *Automatica* 2002, **38**(4):585-596.

[16] Albu-Schffer A, Ott C, Hirzinger G. A Unified Passivity-based Control Framework for Position, Torque and Impedance Control of Flexible Joint Robots. *International Journal of Robotics Research* 2007; **26**(1):23-39.

[17] Fujita M, Kawai H, Spong MW. Passivity-Based Dynamic Visual Feedback Control for Three-Dimensional Target Tracking: Stability and L2-Gain Performance Analysis. *IEEE Transactions on Control Systems Technology* 2007; **15**(1):40-52.

[18] Murakami T, Yu F, Ohnishi K. Torque sensorless control in multidegree-of-freedom manipulator. *IEEE Transactions on Industrial Electronics* 1993; **40**(2):259-265.

[19] Chan SP. A disturbance observer for robot manipulators with application to electronic components assembly. *IEEE Transactions on Industrial Electronics* 1995; **42**(5):487-493.

[20] Komada S, Machii N, Hori T. Control of redundant manipulators considering order of disturbance observer. *IEEE Transactions on Industrial Electronics* 2000; **47**(2):413-420

[21] Chen WH, Ballance DJ, Gawthrop PJ, O'Reilly J. A nonlinear disturbance observer for robotic manipulators. *IEEE Transactions on Industrial Electronics* 2000; **47**(4):932-938

[22] Kolhe JP, Shaheed M, Chandar TS, Talole SE. Robust control of robot manipulators based on uncertainty and disturbance estimation. *The International Journal of Robust and Nonlinear Control* 2013; **23**:104-122.

[23] Lichiardopol S, van de Wouw N, Nijmeijer H. Robust disturbance estimation for humanrobotic comanipulation. *The International Journal of Robust and Nonlinear Control* 2013.

[24] Yao B, Tomizuka M. Smooth robust adaptive sliding mode control of robot manipulators with guaranteed transient performance. *Proceedings of American Control Conference* 1994; 1176-1180.

[25] Yao B, Tomizuka M. Adaptive robust control of SISO nonlinear systems in a semi-strict feedback form. *Automatica* 1997; **33**(5):893-900.

[26] Yao B, Tomizuka M. Adaptive robust control of MIMO nonlinear systems in semi-strict-feedback forms. *Automatica* 2001; **37**(9):1305-1321.

[27] Xie WF. Sliding-Mode-Observer-Based Adaptive Control for Servo Actuator With Friction. *IEEE Transactions on Industrial Electronics* 2007; **54**(3):1517-1527.

[28] Slotine JJE. The robust control of robot manipulators. *International Journal of Robotics Research* 1985; **4**(2):49-63.

[29] Swaroop D, Hedrick JK, Yip PP, Gerdes JC. Dynamic surface control for a class of nonlinear systems. *IEEE Transactions on Automatic Control* 2000; **45**(10):1893-1899.

[30] Young KD, Utkin VI, Ozguner U. A control engineers guide to sliding mode control. *IEEE Transactions on Control Systems Technology* 1999, **7**(3):328-342.

[31] Hovakimyan N, Cao C, Kharisov E, Xargay E, Gregory IM. $\mathcal{L}_1$ adaptive control for safety-critical systems: Guaranteed robustness with fast adaptation. *IEEE Control Systems Magazine* 2011; **5**:54-106.

[32] Yao B. Adaptive robust control of nonlinear systems with application to control of mechanical systems. Ph.D.thesis, Mechanical Engineering Department, University of California at Berkeley, Berkeley, USA, January 1996.

[33] Cao C, Hovakimyan N. Design and Analysis of a Novel $\mathcal{L}_1$ Adaptive Control Architecture With Guaranteed Transient Performance. *IEEE Transactions on Automatic Control* 2008; **53**(2):586-591.

[34] Cao C, Hovakimyan N. Stability Margins of $\mathcal{L}_1$ Adaptive Control Architecture. *IEEE Transactions on Automatic Control* 2010; **55**(2):480-487.

[35] Cao C, Hovakimyan N. $\mathcal{L}_1$ Adaptive Output-Feedback Controllers for Non-Strictly-Positive-Real Reference Systems: Missile Longitudinal Autopilot Design. *Journal of Guidance, Control, and Dynamics* 2009; **32**(3):717-726.

[36] Kaminer I, Pascoal A, Xargay E, Cao C, Hovakimyan N, Dobrokhodov V. Path Following for Unmanned Aerial Vehicles Using $\mathcal{L}_1$ Adaptive Augmentation of Commercial Autopilots. *AIAA Journal of Guidance, Control and Dynamics* 2010; **33**(2):550-564.

[37] Wang J, Hovakimyan N, Cao C. Verifiable Adaptive Flight Control: Unmanned Combat Aerial Vehicle and Aerial Refueling. *AIAA Journal of Guidance, Control, and Dynamics* 2010; **33**(1):75-87.

[38] Dobrokhodov V, Kaminer I, Kitsios I, Xargay E, Hovakimyan N, Cao C, Gregory I, Valavani L. Experimental Validation of Adaptive Control: Rohrs' Counterexample in Flight. *AIAA Journal of Guidance, Control and Dynamics* 2011; **34**(5):1311-1328.

[39] Kazerooni H, Steger R, Huang L. Hybrid Control of the Berkeley Lower Extremity Exoskeleton. *The International Journal of Robotics Research* 2006; **25**(5-6):561-573.

[40] Kazerooni H, Chu A, Steger R. That which does not stabilize, will only make us stronger. *The International Journal of Robotics Research* 2007; **26**(1):75-89.

[41] Khalil HK. *Nonlinear Systems*. Prentice-Hall, 2002.

[42] Hovakimyan N., Cao C. $\mathcal{L}_1$ *Adaptive Control Theory: Guaranteed Robustness with Fast Adaptation*. Philadelphia, PA: SIAM, 2010.

[43] Pomet JB, Praly L. Adaptive nonlinear regulation: estimation from the Lyapunov equation. *IEEE Transactions on Automatic Control* 1992; **37**6:729-740.

[44] Kharisov E, Hovakimyan N, Astrom K. Comparison of Several Adaptive Controllers According to Their Robustness Metrics, *Proceedings of AIAA Guidance, Navigation and Control Conference* 2010; AIAA-2010-8047, Toronto, Canada.

[45] Nguyen KD, Dankowicz H, Hovakimyan N. Marginal Stability in $\mathcal{L}_1$-Adaptive Control of Manipulators. *Proceedings of the 9th International Conference on Multibody Systems, Nonlinear Dynamics, and Control* 2013; DETC2013-12744, Portland, Oregon.